Published in final edited form as:
Nature. 2011 February 10; 470(7333): 274–278. doi:10.1038/nature09625.

Structures of APC/C^{Cdh1} with substrates identify Cdh1 and Apc10 as the D-box co-receptor

Paula C.A. da Fonseca[*,#], **Eric H. Kong**[*,#], **Ziguo Zhang**[*], **Anne Schreiber**[*], **Mark. A. Williams**[‡], **Edward P. Morris**[*], and **David Barford**[*]

[*]Section of Structural Biology, Institute of Cancer Research, Chester Beatty Laboratories, 237 Fulham Road, London, SW3 6JB, UK

[‡]Institute of Structural and Molecular Biology, Department of Biological Sciences, Birkbeck, University of London, Malet Street, London, WC1E 7HX, UK

Abstract

The ubiquitylation of cell cycle regulatory proteins by the large multimeric anaphase promoting complex (APC/C) controls sister chromatid segregation and the exit from mitosis [1,2]. Selection of APC/C targets is achieved through recognition of destruction motifs, predominantly the D-box [3] and KEN-box [4]. Although this process is known to involve a co-activator protein (either Cdc20 or Cdh1) together with core APC/C subunits [1,2], the structural basis for substrate recognition and ubiquitylation is not understood. Here, we investigated the APC/C using single particle electron microscopy (EM) and determined a cryo-EM map of APC/C^{Cdh1} bound to a D-box peptide at ~10 Å resolution. We find that a combined catalytic and substrate recognition module is located within the central cavity of the APC/C assembled from Cdh1, Apc10 - a core APC/C subunit previously implicated in substrate recognition [5,6,7], and the cullin domain of Apc2. Cdh1 and Apc10, identified from difference maps, create a co-receptor for D-box following repositioning of Cdh1 towards Apc10. Using NMR spectroscopy we demonstrate specific D-box – Apc10 interactions, consistent with a role for Apc10 in directly contributing towards D-box recognition by the APC/C^{Cdh1} complex. Our results rationalise the contribution of both co-activator and core APC/C subunits to D-box recognition [8,9] and provide a structural framework for understanding mechanisms of substrate recognition and catalysis by the APC/C.

The APC/C is a multimeric E3 ubiquitin ligase assembled from 13 individual subunits [1,2]. Many of the APC/C's core proteins are comprised of multiple repeat motifs whose principle function is to provide a molecular scaffold, but whose exact biological role is not well understood. The best characterised APC/C subunits are the cullin and RING proteins Apc2 and Apc11 responsible for catalytic activity, and the TPR subunit Apc3/Cdc27 that interacts with co-activator (either Cdc20 or Cdh1) [10,11,12] and the APC/C subunit Apc10 (also known as Doc1) [13]. Both co-activator [9,11,14,15,16,17], and core APC/C subunits [5,6,7,8,9] have been implicated in substrate recognition, but the structural basis for this process is unknown. To

Correspondence and requests for materials should be addressed to D.B. (david.barford@icr.ac.uk)..

Author contributions. All authors contributed to experimental design, data analysis and manuscript preparation. PCAF and EHK collected and analysed EM data, EHK prepared APC/C samples and performed ubiquitylation assays. PCAF determined the 3D EM reconstructions and fitted coordinates. MAW performed NMR experiments and analysed NMR data. EPM helped collect and analyse EM data.

Author information. EM maps have been deposited in EMDB with accession numbers: EMD-1815 (cryo-EM APC/C$^{Cdh1\cdot D\text{-}box}$), EMD-1816 (apo APC/C), EMD-1817 (APC/C^{Cdh1}), EMD-1818 (APC/C$^{Cdh1\cdot KEN\text{-}box}$), EMD-1819 (APC/C$^{Cdh1\cdot Hsl1}$).

[#]These authors contributed equally to this work.

Supplementary Information accompanies the paper on www.nature.com/nature

The authors declare no competing financial interests.

Europe PMC Funders Author Manuscripts

address this question, we used single particle electron microscopy to determine structures of budding yeast APC/C in complex with Cdh1 (APC/C^{Cdh1}) and substrates. The resultant EM maps are of exceptional quality and detail. Our new maps show the characteristic triangular shape of the APC/C [18,19,20,21] (Supplementary Fig. 1), but at higher resolution we visualise a lattice-like scaffold assembled from individual APC/C subunits defining a central cavity.

The APC/C co-activator Cdh1 was identified in negative stain EM reconstructions as a prominent and discrete density feature present within the central cavity of APC/C^{Cdh1} and absent from APC/C (Fig. 1a,b). Its disc-shaped density, characteristic of an exposed WD40 β-propeller domain, is connected to the APC/C via an edge-on interface. Overall, with the exception of the Cdh1 density, APC/C and APC/C^{Cdh1} are similar, and the large conformational changes that accompany co-activator binding to vertebrate APC/C [19,21] are not evident. An ellipsoid-shaped density feature, resembling the β-sandwich of Apc10 [13,22], situated adjacent to, but not in contact with Cdh1, is more prominent in the presence of Cdh1 (Fig. 1a,b). Its close proximity to Cdh1 was intriguing in view of the role of Apc10 in contributing towards substrate recognition [6], and the D-box-dependent processivity of the ubiquitylation reaction [5,7]. To unequivocally identify Apc10, we generated APC/C$^{\Delta Apc10}$ in complex with Cdh1 (APC/C$^{\Delta Apc10\text{-}Cdh1}$). The resultant APC/C$^{\Delta Apc10\text{-}Cdh1}$ map showed complete loss of this ellipsoid density (Fig. 1c), confirming its identity as Apc10. Deletion of Apc10 also resulted in a depletion of Cdh1 density around the circumference of the β-propeller most distant from its contact to APC/C (Fig. 1c). Since deletion of Apc10 does not affect the APC/C subunit composition [6] or abrogate Cdh1 binding (Supplementary Fig. 2), the partial loss of Cdh1 density is indicative of an increased flexibility of Cdh1's WD40 domain. This finding and the reduced density for Apc10 in APC/C imply conformational interdependence of Apc10 and Cdh1.

To identify substrate-binding sites on APC/C^{Cdh1}, we utilised a fragment of Hsl1, a D-box (RxxLxxI/VxN) [3] and KEN-box (KEN) [4] containing substrate with high affinity for APC/C^{Cdh1} (refs [14,23]). The ternary APC/C$^{Cdh1\cdot Hsl1}$ complex was catalytically competent, as judged by its ability to ubiquitylate Hsl1 (Supplementary Fig. 3a). Engagement of Hs1l with APC/C^{Cdh1} is accompanied by a pronounced structural change involving Cdh1 and Apc10 (Fig. 1d). Specifically, the β-propeller domain of Cdh1 is bulkier, shifts ~7 Å towards Apc10, and new, well-defined density bridges Cdh1 to Apc10. Thus, Hsl1 promotes the formation of new connections between Cdh1 and Apc10, a result consistent with direct co-activator - substrate interactions [9,11,14,15,16,17] and a role for Apc10 in mediating optimal substrate binding [5,6,7,23].

To define the specific roles of the D- and KEN-boxes in contributing to these conformational changes, we determined structures of APC/C^{Cdh1} in complex with synthetic peptides containing either a D-box or a KEN-box. Similar to previous results with D-box peptides [11,24], an 18-residue D-box peptide modelled on cyclin B (*S. pombe* Cdc13) completely inhibited APC/C^{Cdh1} activity towards Clb2 (a mitotic cyclin with D- and KEN-boxes) at 0.1 mM (Supplementary Fig. 4a). Fig. 1e shows that D-box peptide generated similar structural changes to Hsl1, specifically the WD40 domain of Cdh1 is shifted, and new density connects it with Apc10 (Supplementary mov1). However, in contrast to the APC/C$^{Cdh1\cdot Hsl1}$ map, the extent of new density associated with Cdh1 is markedly reduced, suggesting that the additional density in APC/C$^{Cdh1\cdot Hsl1}$ represents the larger Hsl1 substrate. Control experiments show that a mutant D-box peptide, which fails to bind APC/C^{Cdh1} (Supplementary Fig. 4c), induces no conformational changes (Supplementary Fig. 5). Binding of the KEN-box peptide to APC/C^{Cdh1} also promotes a repositioning of Cdh1 towards Apc10, but notably without the connecting density (Fig. 1f). This indicates that only D-box substrates promote a physical interconnection between Cdh1 and Apc10.

To explore the structure of APC/C$^{Cdh1\cdot D\text{-}box}$ in more detail, we collected cryo-EM images of the complex and determined its structure at ~10 Å resolution. The cryo-EM map reproduces the overall features of the APC/C$^{Cdh1\cdot D\text{-}box}$ map generated from negatively stained particles, but with greatly enhanced detail and resolution (Fig. 2, Supplementary Fig. 6,7). Similar to the APC/C$^{Cdh1\cdot D\text{-}box}$ ternary complex obtained from negative stain EM, the cryo-EM reconstruction shows density connecting Cdh1 and Apc10 (Figs. 2,4). Docking the crystal structure of Apc10 (refs [13],[22]) and the modelled Cdh1 WD40 domain into their respective densities, indicates additional unassigned density linking Cdh1 to Apc10 (Fig. 4a,c). Strikingly, the best fit of Apc10 into the cryo-EM map positions a highly conserved loop, required for D-box recognition [7], adjacent to the density linking Apc10 with Cdh1. In contrast, residues on Apc10's opposite surface that contribute to APC/C interactions [7], are oriented towards Apc2 (Fig. 4c).

These structural data revealing that Cdh1 and Apc10 become interconnected by bridging density in the presence of D-box substrates rationalises biochemical studies demonstrating that both co-activator and core APC/C subunits [8],[9],[11],[14],[15],[16],[17], specifically Apc10 [5],[6],[7],[23], contribute to D-box dependent recognition and processive ubiquitylation. The unassigned density bridging Apc10 and Cdh1 in the APC/C$^{Cdh1\cdot D\text{-}box}$ complex can be modelled as a D-box peptide, indicating that the binding site for D-box is shared between the WD40 domain of Cdh1 and the β-sandwich of Apc10. Cdh1 and Apc10 therefore generate a D-box co-receptor (Supplementary Fig. 8). Although biochemical data show that the D-box interacts with the conserved surface of co-activator's WD40 domain [11],[15], direct interactions between D-box and Apc10 alone have not previously been demonstrated (our unpublished data and [7]), possibly due to the weak affinity of isolated Apc10 for D-box.

We used ^{15}N-HSQC NMR, a technique suitable for detecting weak protein-ligand interactions, to investigate potential Apc10 - D-box interactions. The ^{15}N-HSQC NMR spectrum of *S. cerevisiae* Apc10, shown in Fig. 3, has a substantial number of well-dispersed peaks consistent with the Apc10 β-sandwich architecture [22]. However, the number of visible peaks is ~ half that expected for a 221 residue protein, and the visible peaks have a wide range of intensities. Reduced peak number and intensity variation are characteristic of proteins undergoing exchange between different conformational or oligomeric states. Spectra recorded with a two-fold difference in protein concentration showed no change in position or shape of any dispersed peak suggesting there is no sensitivity to any possible oligomerisation equilibrium. Consequently, the features of the ^{15}N-HSQC spectrum are best explained as a result of Apc10 adopting multiple conformations in intermediate to slow exchange (sub-millisecond to second timescales) in solution. Addition of a stoichiometric excess (~40-fold) of the D-box peptide used to generate the APC/C$^{Cdh1\cdot D\text{-}box}$ ternary complex resulted in more than 20 changes in amide peak position or relative intensity (Fig. 3). NMR-based measurement of the translational diffusion coefficient showed that the NMR-observed species is an Apc10 monomer of ~26 kDa. Thus, the changes in specific peaks on addition of peptide demonstrate that the D-box peptide interacts with monomeric Apc10, altering the chemical environment and/or the conformational equilibrium of a subset of its residues. However, the low intensity and proportion of visible amide peaks made sequential assignment and full characterisation of the D-box binding site on Apc10 impracticable.

To establish whether the peptide-induced changes of the Apc10 NMR spectrum are specifically D-box-dependent, we performed a series of control experiments. First, a different D-box peptide (a 19-residue peptide modelled on *S. cerevisiae* Clb2 whose sequence identity with Cdc13 is confined to the D-box) produced very similar NMR spectral changes as the Cdc13 D-box (Fig. 3). Second, a mutant D-box Cdc13 peptide resulted in only minor changes in the Apc10 NMR spectrum, consistent with greatly reduced binding.

Finally, the Hsl1 KEN-box peptide, which from the APC/$C^{Cdh1\cdot KEN\text{-}box}$ EM analysis does not bridge Cdh1 and Apc10, resulted in an essentially identical spectrum to that of the apo-protein, with none of the changes seen for the two D-box containing peptides. These NMR data therefore provide strong evidence for a direct interaction between Apc10 and D-box, supporting the notion that Apc10 participates in D-box recognition.

To gain further insight into the mechanisms of substrate recognition and ubiquitylation, we modelled atomic structures of Apc2 and Cdc27 into the molecular envelope of the APC/$C^{Cdh1\cdot D\text{-}box}$ map. We fitted a homology model of Apc2, based on Cul4a-Rbx1, allowing for small adjustments of the C-terminal domain (CTD) relative to the cullin repeats (Fig. 4, Supplementary Fig. 7,9). Continuous density attaches the globular CTD to that of the cullin repeats, which are seen as a long stalk-like density that transverses one side of the complex (Fig. 4, Supplementary Fig. 7). The APC/$C^{Cdh1\cdot D\text{-}box}$ cryo-map reveals that Cdh1 and Apc10 are both connected to the Apc2 CTD (Fig. 4c, Supplementary Fig. 7). Notably, the interaction of the CTD of Apc2 with substrate adaptor subunits contrasts with the SCF complex in which the N-terminal cullin repeat of Cul1 interacts with substrate adaptors [25].

Cdc27 is a dimer and we docked its N-terminal dimerisation domain [26] into the globular structure at the head of the TPR sub-complex, and independently positioned the modelled C-terminal TPR super-helices of the Cdc27 subunits into the curved tubular densities extending from the globular domain (Fig. 4a,b, Supplementary Fig. 7), consistent with the mapping of Cdc27 (ref. [27]). Although not imposed in the fitting, these docked TPR super-helices are related by the same dyad symmetry as the Cdc27 dimerisation domain, therefore preserving the overall two-fold symmetry of Cdc27 (Fig. 4a). The organisation of Apc2 and Cdc27 in close proximity to Cdh1 and Apc10 visualised in our APC/$C^{Cdh1\cdot D\text{-}box}$ structure unifies previous models of APC/C subunit topologies [10,12,13,23] (Fig. 4d). Cdh1 is known to interact through its C-terminal Ile-Arg (IR) tail with Cdc27 [10,11,12], and in *S. cerevisiae*, Cdh1 also requires Apc2 for optimal binding [12]. The structures fitted to the EM map show that with the C-terminus of Cdh1 in contact with Cdc27, its N-terminal C-box is positioned to contact Apc2 (Fig. 4, Supplementary Fig. 7) [12,17]. Pulldown experiments on recombinant human proteins have shown that Apc10 interacts with Cdc27 through its C-terminal region, which also contains an IR-motif [13], whereas in *S. cerevisiae*, Apc10 associates preferentially with a sub-complex of Apc1, Apc2 and Apc11 (ref. [12]). Our EM data position Apc10 close to the second Cdc27 subunit. Consequently, the human and yeast biochemical data are explained by the extensive interface between Apc10 and Apc2, and the flexible C-terminal IR-tail of Apc10 binding to the Cdc27 TPR super-helix.

This study identifies Cdh1 and Apc10 as a co-receptor for D-box. Individually, co-activator and APC/C possess low affinity and specificity for substrate [9] and therefore cooperatively enhances substrate affinity through multivalency. Definition of the subunit organisation and generation of a pseudo-atomic structure of the APC/C [27], together with characterisation of the D-box co-receptor presented here, provide the conceptual framework for a mechanistic understanding of the APC/C.

Methods Summary

Generation of APC/C and complexes with Cdh1 and substrates

APC/C and APC/$C^{\Delta Apc10}$ were isolated from *S. cerevisiae* and ubiquitylation assays were performed essentially as described [6]. *S. cerevisiae* His_6-Cdh1 was expressed in *Sf*9 cells and purified using Ni-NTA. APC/C^{Cdh1} was prepared by loading excess Cdh1 to APC/C immobilised on calmodulin resin, and eluted as for APC/C. APC/C^{Cdh1}-substrate complexes were generated as described in Methods.

Electron microscopy and image analysis

Purified APC/C (~0.2 mg/ml) from peak elution fractions was applied to Quantifoil 1.2 or 2 μm aperture grids coated with continuous thin carbon and either negatively stained for electron microscopy at room temperature or flash frozen using a Vitrobot for cryo-EM. Images were recorded in an FEI TF20 electron microscope under low dose conditions using a Tietz F415 CCD camera. Three-dimensional maps were calculated from molecular images using programs from Imagic [28], Spider [29] and EMAN [30].

NMR analysis

^{1}H-^{15}N HSQC spectra were recorded at 25°C over 5.5 or 11 hours for samples of Apc10 alone and in the presence of four peptides samples using a (^{1}H,^{15}N,^{13}C) triple resonance cryoprobe on a 700MHz Bruker Avance III spectrometer. Spectra were processed identically and displayed to compensate for concentration and/or recording time differences.

Supplementary Material

Refer to Web version on PubMed Central for supplementary material.

Acknowledgments

This work was funded by a Cancer Research UK grant to DB. We thank Fabienne Beuron for help with early stages of this project and for EM support, and the assistance of John Kirkpatrick and the facilities of the UCL/Birkbeck ISMB Biomolecular NMR Centre.

Appendix

Methods

Generation of APC/C and complexes with Cdh1 and substrates

APC/C and APC/$C^{\Delta Apc10}$ were isolated from *S. cerevisiae* and ubiquitylation assays were performed as described [6,31] except that the calmodulin resin elution buffer was 25 mM HEPES (pH 8.0), 150 mM NaCl, 1 mM MgCl, 2 mM EGTA, 3 mM TCEP, 0.03% (v/v)), n-Dodecyl β-D-maltoside (DDM). Peak elution fractions were used for EM analysis. *S. cerevisiae* His_6-Cdh1 was expressed in *Sf*9 cells and purified using Ni-NTA. APC/C^{Cdh1} was prepared by loading excess Cdh1 to APC/C immobilised on calmodulin resin, thereby ensuing formation of a stoichiometric APC/C^{Cdh1} complex, and eluted as for APC/C. Association of Cdh1 to APC/C was confirmed by SDS PAGE and Western blotting analyses (Supplementary Fig. 2), and by E3 ligase assays showing APC/C^{Cdh1} ubiquitylated Hsl1 and Clb2 (Supplementary Fig. 3,4). $Hsl1^{667-872}$ was expressed in BL21(DE3) RIL cells and purified by Ni-NTA and gel filtration chromatography and added to APC/C^{Cdh1} to a final concentration of 1.5 μM for EM data collection, greatly in excess of the APC/C^{Cdh1} concentration (Supplementary Fig. 3a). Previous work from Morgan's laboratory had shown that Hsl1 forms a stable 1:1 complex with APC/C^{Cdh1} at ~0.05 μM [23]. APC/$C^{Cdh1\cdot Hsl1}$ was completely inhibited towards Clb2 (Supplementary Fig. 3b). D-box peptide inhibited APC/C^{Cdh1} ubiquitylation of Clb2 at 0.1 mM (Supplementary Fig. 4a), similar to previous findings [11,24]. APC/$C^{Cdh1\cdot D\text{-}box}$ and APC/$C^{Cdh1\cdot mutD\text{-}box}$ were prepared by adding peptide to APC/C^{Cdh1} to a final concentration of 0.3 mM. KEN-box peptide inhibited APC/C^{Cdh1} ubiquitylation of Clb2 at 1 mM (Supplementary Fig. 4b) and was therefore used at 10 mM for the APC/$C^{Cdh1\cdot KEN\text{-}box}$ structure. Peptides used in the EM structural analysis and ubiquitylation assays were as follows. D-box: NVPKKRHALDDVSNFHNK, mutD-box: NVPKKAHAADDVSAFHNK, KEN-box: GVSTNKENEGPEYPTKIKKEHQK (D-box, mutant D-box and KEN-box underlined). D box and KEN box peptides modelled on *S. pombe* Cdc13 and *S. cerevisiae* Hsl1, respectively. Stock solutions were dissolved at 10-20

Europe PMC Funders Author Manuscripts

mM in 100 mM Tris.HCl (pH 8.0). For competitions assays, peptides were used at the final stated concentrations.

Electron microscopy of negative stained samples

Purified APC/C and its Cdh1 and substrate complexes at ~0.2 mg/ml were applied to Quantifoil 2/2 EM grids coated with a second layer of thin carbon. The grids were negatively stained with 2% (w/v) uranyl acetate. The samples were imaged at room temperature in a FEI Tecnai TF20 electron microscope at an accelerating voltage of 200 kV, in low dose mode with an exposure of ~100 $e^{-}/Å^2$, a nominal magnification of 50,000x and an underfocus of ~1.2 μm, giving rise to a first minimum in the contrast transfer function at ~17 Å. Images were recorded using a Tietz F415 (4k × 4k) CCD camera and adjacent boxes of 2×2 pixels were averaged, resulting in a calibrated sampling of 3.47 Å/pixel. The images recorded for all negatively stained samples were consistent with that of APC/C^{Cdh1} shown in Supplementary Fig. 10a, including those of samples of $APC/C^{\Delta Apc10\cdot Cdh1}$ (Supplementary Fig.11).

Cryo-EM

Samples of purified $APC/C^{Cdh1\cdot D\text{-}box}$ were applied to Quantifoil 1.2/1.3 EM grids coated with a second layer of thin carbon, blotted and plunged into liquid ethane using an FEI Vitrobot. The grids were transferred into a Tecnai TF20 and maintained at approximately −178 °C using a Gatan 626 cryo-holder. Images were recorded in a similar way to that described for negatively stained samples, except that focal pairs were recorded at an underfocus of ~2.5 μm and ~4 μm, using an electron dose of ~20 $e^{-}/Å^2$ (for each exposure) and a nominal magnification of 63,000x, resulting in a sampling of 2.82 Å/pixel. The first recorded CCD images of each focal pair (closer to focus) were carefully screened and only those with a power spectrum showing Thon rings extending isotropically beyond 10 Å were selected for further analysis.

Image analysis of negatively stained samples

Image processing was performed using Imagic [28], Spider [29] and EMAN [30] programs. Image processing was initiated with the analysis of the APC/C^{cdh1} complex. Molecular images were manually selected (Supplementary Fig. 10a) using the EMAN boxer software in order to assemble a dataset ultimately formed of 12,529 images. A preliminary evaluation of the resulting dataset was carried out by calculating reference-free image class-averages using the refine2d routine from EMAN. Three classes, which were judged to be approximately mutually orthogonal, were selected from the preliminary set for angular assignment using the Imagic C1 start-up procedure. These were used to assign angles, by angular reconstitution, to a further selection of 112 classes, which were subsequently back-projected in order to create an *ab initio* 3D map. This map was used as the first reference for refinement using a combination of Imagic and Spider software. The refinement consisted of multiple rounds of multi-reference alignment, classification, angular assignment (to selected image-class averages) by projection matching and 3D reconstruction by back-projection. In the last round of refinement a total of 4,000 class-averages were calculated, of which 1,433 were selected to calculate the final 3D map. Examples of class-averages used in the reconstruction and their respective reprojections are shown in Supplementary Fig. 10b. The angular distribution of the classes used in the final reconstruction is shown in Supplementary Fig. 10c. The resolution of the final map of APC/C^{Cdh1} was estimated by Fourier shell correlation as 18-20 Å, depending on the resolution criteria (Supplementary Fig. 10d). Negatively stained $APC/C^{\Delta Apc10\cdot Cdh1}$ appear indistinguishable from APC/C^{Cdh1} (Supplementary Fig. 11).

Europe PMC Funders Author Manuscripts

The final map calculated for APC/C^{cdh1} was used as a starting reference for the analysis of all other negatively stained APC/C complexes, followed by the same refinement procedures. The total number of molecular images used in the image analysis of each sample is summarised in Supplementary Table 1. Representations of the maps were generated using PyMOL (www.pymol.org).

Image analysis of data from cryo-EM

The CTF was measured for each CCD image selected for analysis and corrected by phase reversal. A dataset of 9474 molecular images of the APC/C$^{Cdh1\cdot D\text{-}box}$ complex was assembled manually using the EMAN boxer software, from the first recorded CCD image of each focal pair (closer to focus, Supplementary Fig. 12a), using the higher contrast second image as an aid for the selection. The subsequent analysis was performed using Imagic and Spider software. The map of the APC/C$^{Cdh1\cdot D\text{-}box}$ complex determined by the analysis of negatively stained samples was used as a starting reference for the analysis. The molecular images were aligned and their angular assignment performed by projection matching against the initial reference map. A first 3D reconstruction was calculated by back-projection and this was further refined by multiple rounds of alignment, angular assignment by projection matching and back-projection. The angular distribution of the images for the calculation of the final map is shown in Supplementary Fig. 12b. The resolution of the final map, estimated by Fourier shell correlation, is 9-10 Å, depending on the resolution criteria (Supplementary Fig. 12c). For the representation of the final reconstruction a reverse B-factor of -300 was applied, in order to optimise the agreement between the resulting reconstruction and the fitted coordinates, followed by a Fourier low-pass filtration to 9.5 Å. PyMOL (www.pymol.org) was used to generate the representations of the map.

Fitting atomic coordinates to cryo-EM map of APC/C$^{Cdh1\cdot D\text{-}box}$

Apc10 based on *S. cerevisiae* Apc10/Doc1 (PDB code 1GQP) [22], N-terminal dimerisation domain of Cdc27 based on *E. cuniculi* Cdc27 (PDB code 3KAE) [26] and C-terminal TPR super-helix are based on model of [26] (overall sequence identity of 16%). *S. cerevisiae* Cdh1 and Apc2 were modelled using the PHYRE server [32] based on coordinates PDB codes 2GNQ (WDR5) [33] and 2HYE (Cul4a-Rbx1) [34] respectively, with overall sequence identities of 17% and 11%).

Atomic coordinates of Apc10 (PDB 1GQP) and the N-terminal homo-dimerisation domain of Cdc27 (PDB 3KAE) and the molecular models of Cdh1, Apc2 (cullin domain and cullin repeats independently) and two copies of the model of the C-terminal TPR repeats of Cdc27 were docked into the cryo-EM map of the APC/C$^{Cdh1\cdot D\text{-}box}$ complex using URO software [35] (correlation coefficient of 0.82). The fitted coordinates were converted to densities, Fourier low-pass filtered to 9.5 Å and rendered to yield a volume corresponding to their calculated molecular mass, of 243 kDa, assuming a protein density of 0.844 Da/Å ^{3}. The filtered coordinates were used to guide the rendering of the APC/C$^{Cdh1\cdot D\text{-}box}$ map, resulting in a volume corresponding to ~1.13 MDa. Furthermore, the comparison of the level of detail shown by the docked coordinates and that in our 3D map of APC/C$^{Cdh1\cdot D\text{-}box}$, determined from cryo-EM data, is supportive of a resolution estimate of ~10 Å (Supplementary Fig. 7).

The protocol by which the *ab initio* APC/C^{Cdh1} map was calculated, which was the initial reference for the analysis of all complexes presented here, results in 3D maps with ambiguity with respect to their hand. However, the hand of the APC/C complex as presented here has been previously determined by random conical tilt methods [19,21]. In the present work the hand shown is supported by the agreement between the docked coordinates and their respective densities.

NMR analysis

Uniformly ^{15}N-labelled Apc10 was purified from *E. coli* grown in a defined minimal medium supplemented with ^{15}N-ammonium sulphate using constructs and protocols previously described [22]. Peptides (Supplementary Table 2) were dissolved in 100 mM Tris/MOPS to the lower of the limit of either their maximum solubility or a 100 mM concentration, and their pH adjusted to ~8 with NaOH. Peptide was added to protein stock to a final concentration of 5 mM. Protein solubility and propensity to aggregation determined the optimal solution conditions for NMR data collection. All NMR samples were in 90% H_2O:10% D_2O, 77-85 mM NaCl, 4.5 mM DTT, 90 mM Tris/Mops buffer pH 8.0. For the spectra shown, with the exception of the Clb2 sample, final protein concentration was 130-160 μM. Addition of the Clb2 D-box-containing peptide caused substantial precipitation of the protein (also seen to a lesser degree with the Cdc13 D-box peptide), leading to a final protein concentration in this sample of 64 μM. The pH of final protein:peptide mixtures was confirmed by NMR chemical shift of Tris methylene peaks [36] to be 8.0 ± 0.1. The Hsl1 KEN-box peptide used for NMR studies inhibited APC/C^{Cdh1}-catalysed ubiquitylation of Clb2 at a concentration of 2 mM (data not shown).

^{1}H-^{15}N HSQC spectra of 1024×128 complex points were recorded for each sample using a (^{1}H,^{15}N,^{13}C) triple resonance cryoprobe on a 700 MHz Bruker Avance III spectrometer with identical spectral widths. Data were recorded at 25°C for 5.5 or 11 h. The same spectral processing was applied to each spectrum (Gaussian apodisation in ^{1}H and sine-bell apodisation in ^{15}N dimensions and zero filling to 2048×512 points before Fourier transformation and polynomial baseline correction) using NmrPipe [37]. Spectra were overlaid in CCPNmr Analysis [38] and contour levels matched for concentration and recording time differences using the intense peaks common to all five spectra.

The field-gradient dependence of the signal intensity of the central region of the ^{15}N-edited spectrum (containing the strongest signals) of the APC10 with the Cdc13 D-box peptide was used to measure the extent of translational diffusion during a fixed time interval [39]. The data fit a model corresponding to a single species of molecular mass ~26 kDa, i.e. that of the monomer, with no indication of a significant NMR-observable population of dimer or higher order oligomers.

References

31. Passmore LA, Barford D, Harper JW. Purification and assay of the budding yeast anaphase-promoting complex. Methods Enzymol. 2005; 398:195–219. [PubMed: 16275330]
32. Kelley LA, Sternberg MJ. Protein structure prediction on the Web: a case study using the Phyre server. Nat Protoc. 2009; 4:363–371. [PubMed: 19247286]
33. Schuetz A, et al. Structural basis for molecular recognition and presentation of histone H3 by WDR5. EMBO J. 2006; 25:4245–4252. [PubMed: 16946699]
34. Angers S, et al. Molecular architecture and assembly of the DDB1-CUL4A ubiquitin ligase machinery. Nature. 2006; 443:590–593. [PubMed: 16964240]
35. Navaza J, Lepault J, Rey FA, Alvarez-Rua C, Borge J. On the fitting of model electron densities into EM reconstructions: a reciprocal-space formulation. Acta Crystallogr D Biol Crystallogr. 2002; 58:1820–1825. [PubMed: 12351826]
36. Baryshnikova OK, Williams TC, Sykes BD. Internal pH indicators for biomolecular NMR. J Biomol NMR. 2008; 41:5–7. [PubMed: 18398685]
37. Delaglio F, et al. NMRPipe: a multidimensional spectral processing system based on UNIX pipes. J Biomol NMR. 1995; 6:277–293. [PubMed: 8520220]
38. Vranken WF, et al. The CCPN data model for NMR spectroscopy: development of a software pipeline. Proteins. 2005; 59:687–696. doi:10.1002/prot.20449. [PubMed: 15815974]

39. Wu D, Chen A, Johnson CS Jr. An Improved Diffusion-Ordered Spectroscopy Experiment Incorporating Bipolar-Gradient Pulses. J. Magn. Reson. 1995; A115:260–264.

References

1. Peters JM. The anaphase promoting complex/cyclosome: a machine designed to destroy. Nat Rev Mol Cell Biol. 2006; 7:644–656. [PubMed: 16896351]
2. Thornton BR, Toczyski DP. Precise destruction: an emerging picture of the APC. Genes Dev. 2006; 20:3069–3078. [PubMed: 17114580]
3. Glotzer M, Murray AW, Kirschner MW. Cyclin is degraded by the ubiquitin pathway. Nature. 1991; 349:132–138. [PubMed: 1846030]
4. Pfleger CM, Kirschner MW. The KEN box: an APC recognition signal distinct from the D box targeted by Cdh1. Genes Dev. 2000; 14:655–665. [PubMed: 10733526]
5. Carroll CW, Morgan DO. The Doc1 subunit is a processivity factor for the anaphase-promoting complex. Nat Cell Biol. 2002; 4:880–887. [PubMed: 12402045]
6. Passmore LA, et al. Doc1 mediates the activity of the anaphase-promoting complex by contributing to substrate recognition. Embo J. 2003; 22:786–796. [PubMed: 12574115]
7. Carroll CW, Enquist-Newman M, Morgan DO. The APC subunit Doc1 promotes recognition of the substrate destruction box. Curr Biol. 2005; 15:11–18. [PubMed: 15649358]
8. Yamano H, Gannon J, Mahbubani H, Hunt T. Cell cycle-regulated recognition of the destruction box of cyclin B by the APC/C in Xenopus egg extracts. Mol Cell. 2004; 13:137–147. [PubMed: 14731401]
9. Eytan E, Moshe Y, Braunstein I, Hershko A. Roles of the anaphase-promoting complex/cyclosome and of its activator Cdc20 in functional substrate binding. Proc Natl Acad Sci U S A. 2006; 103:2081–2086. [PubMed: 16455800]
10. Vodermaier HC, Gieffers C, Maurer-Stroh S, Eisenhaber F, Peters JM. TPR subunits of the anaphase-promoting complex mediate binding to the activator protein CDH1. Curr Biol. 2003; 13:1459–1468. [PubMed: 12956947]
11. Kraft C, Vodermaier HC, Maurer-Stroh S, Eisenhaber F, Peters JM. The WD40 propeller domain of Cdh1 functions as a destruction box receptor for APC/C substrates. Mol Cell. 2005; 18:543–553. [PubMed: 15916961]
12. Thornton BR, et al. An architectural map of the anaphase-promoting complex. Genes Dev. 2006; 20:449–460. [PubMed: 16481473]
13. Wendt KS, et al. Crystal structure of the APC10/DOC1 subunit of the human anaphase-promoting complex. Nat Struct Biol. 2001; 8:784–788. [PubMed: 11524682]
14. Burton JL, Solomon MJ. D box and KEN box motifs in budding yeast Hsl1p are required for APC-mediated degradation and direct binding to Cdc20p and Cdh1p. Genes Dev. 2001; 15:2381–2395. [PubMed: 11562348]
15. Hilioti Z, Chung YS, Mochizuki Y, Hardy CF, Cohen-Fix O. The anaphase inhibitor Pds1 binds to the APC/C-associated protein Cdc20 in a destruction box-dependent manner. Curr Biol. 2001; 11:1347–1352. [PubMed: 11553328]
16. Pfleger CM, Lee E, Kirschner MW. Substrate recognition by the Cdc20 and Cdh1 components of the anaphase-promoting complex. Genes Dev. 2001; 15:2396–2407. [PubMed: 11562349]
17. Schwab M, Neutzner M, Mocker D, Seufert W. Yeast Hct1 recognizes the mitotic cyclin Clb2 and other substrates of the ubiquitin ligase APC. Embo J. 2001; 20:5165–5175. [PubMed: 11566880]
18. Passmore LA, et al. Structural analysis of the anaphase-promoting complex reveals multiple active sites and insights into polyubiquitylation. Mol Cell. 2005; 20:855–866. [PubMed: 16364911]
19. Dube P, et al. Localization of the coactivator Cdh1 and the cullin subunit Apc2 in a cryo-electron microscopy model of vertebrate APC/C. Mol Cell. 2005; 20:867–879. [PubMed: 16364912]
20. Ohi MD, et al. Structural organization of the anaphase-promoting complex bound to the mitotic activator Slp1. Mol Cell. 2007; 28:871–885. [PubMed: 18082611]
21. Herzog F, et al. Structure of the anaphase-promoting complex/cyclosome interacting with a mitotic checkpoint complex. Science. 2009; 323:1477–1481. [PubMed: 19286556]

22. Au SW, Leng X, Harper JW, Barford D. Implications for the ubiquitination reaction of the anaphase-promoting complex from the crystal structure of the Doc1/Apc10 subunit. J Mol Biol. 2002; 316:955–968. [PubMed: 11884135]
23. Matyskiela ME, Morgan DO. Analysis of activator-binding sites on the APC/C supports a cooperative substrate-binding mechanism. Mol Cell. 2009; 34:68–80. [PubMed: 19362536]
24. Yamano H, Tsurumi C, Gannon J, Hunt T. The role of the destruction box and its neighbouring lysine residues in cyclin B for anaphase ubiquitin-dependent proteolysis in fission yeast: defining the D-box receptor. Embo J. 1998; 17:5670–5678. [PubMed: 9755167]
25. Zheng N, et al. Structure of the Cul1-Rbx1-Skp1-F boxSkp2 SCF ubiquitin ligase complex. Nature. 2002; 416:703–709. [PubMed: 11961546]
26. Zhang Z, et al. Molecular structure of the N-terminal domain of the APC/C subunit Cdc27 reveals a homo-dimeric tetratricopeptide repeat architecture. J Mol Biol. 2010; 397:1316–1328. [PubMed: 20206185]
27. Schreiber A, et al. Structural basis for the subunit assembly of the anaphase promoting complex. Submitted.
28. van Heel M, et al. Single-particle electron cryo-microscopy: towards atomic resolution. Q Rev Biophys. 2000; 33:307–369. [PubMed: 11233408]
29. Frank J, et al. SPIDER and WEB: processing and visualization of images in 3D electron microscopy and related fields. J Struct Biol. 1996; 116:190–199. [PubMed: 8742743]
30. Ludtke SJ, Baldwin PR, Chiu W. EMAN: semiautomated software for high-resolution single-particle reconstructions. J Struct Biol. 1999; 128:82–97. [PubMed: 10600563]

Europe PMC Funders Author Manuscripts

Europe PMC Funders Author Manuscripts

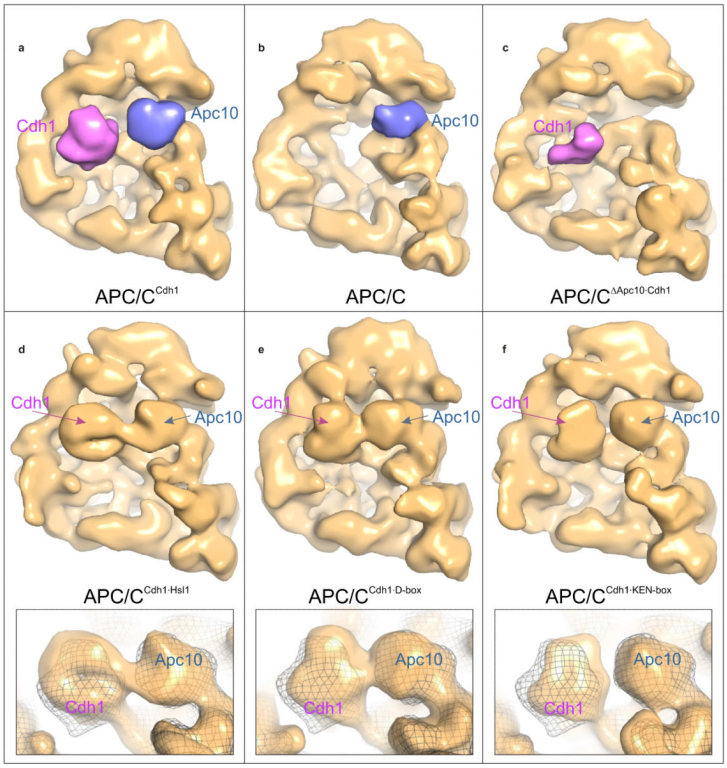

Figure 1.

Negative stain electron microscopy reconstructions of budding yeast APC/C show that substrate binding to APC/C^{Cdh1} involves Cdh1 and Apc10. (a) APC/C^{Cdh1}, (b) APC/C, (c) APC/$C^{\Delta Apc10\cdot Cdh1}$. Density assigned to Cdh1 and Apc10 is shown in magenta and blue, respectively. The resolution of the APC/C^{Cdh1} binary complex is ~18-20 Å (Supplementary Fig. 10d). Negative stain EM reconstructions of (d) APC/$C^{Cdh1\cdot Hsl1}$ complex, (e) APC/$C^{Cdh1\cdot D\text{-}box}$, (f) APC/$C^{Cdh1\cdot KEN\text{-}box}$. Lower panels in (d), (e) and (f) show details of the structural changes associated with Cdh1 and Apc10 in the presence of substrate compared with the superimposed binary APC/C^{Cdh1} map represented in mesh. Hsl1 and D-box and KEN-box peptides were used at saturating concentrations to promote stoichiometric APC/C^{Cdh1}-substrate ternary complexes.

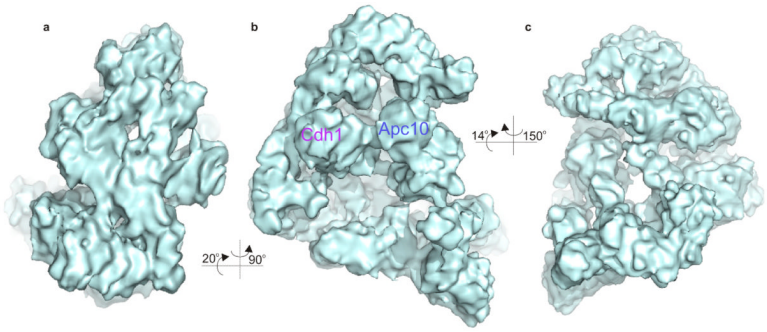

Figure 2.

Cryo-electron microscopy reconstruction of budding yeast APC/C$^{Cdh1\cdot D\text{-}box}$ reveals the lattice-like architecture of the complex. Three views of the complex with (b) similar to views shown in figure 1. Resolution is ~10 Å (Supplementary Fig. 12c).

Europe PMC Funders Author Manuscripts

Europe PMC Funders Author Manuscripts

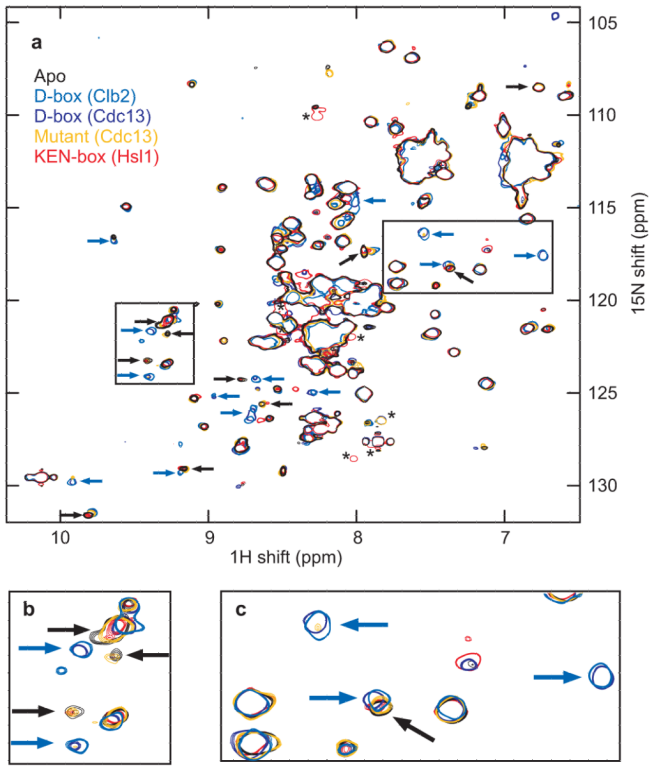

Figure 3.

^{1}H-^{15}N HSQC spectra of Apc10. Overlaid are spectra of the apo-protein and protein in the presence of stoichiometric excess of each of four peptides. The complete amide region (a) and for clarity expanded views of two boxed sub-regions (b, c) are shown. Spectra in the presence of either of the two D-box containing peptides show common changes with respect to the apo-protein spectrum, namely absence of the peaks seen in the apo-protein (black arrows) and new or shifted peaks not seen in the apo-spectrum (blue arrows). In contrast, spectra in the presence of either the Cdc13-derived peptide in which four residues of the D-box motif are mutated to alanine or a peptide containing a KEN-box motif are very similar to the apo-spectrum, retaining all of the peaks marked by black arrows. The spectrum with the mutant Cdc13 peptide does in some cases show low intensity peaks at the positions indicated by blue arrows (see expanded views b, c) indicating a very weak residual interaction. These spectra are consistent with a D-box dependent interaction with Apc10. (Peaks arising from natural abundance ^{15}N amides in the unbound peptide that are protected from solvent exchange are indicated by an asterisk).

Europe PMC Funders Author Manuscripts

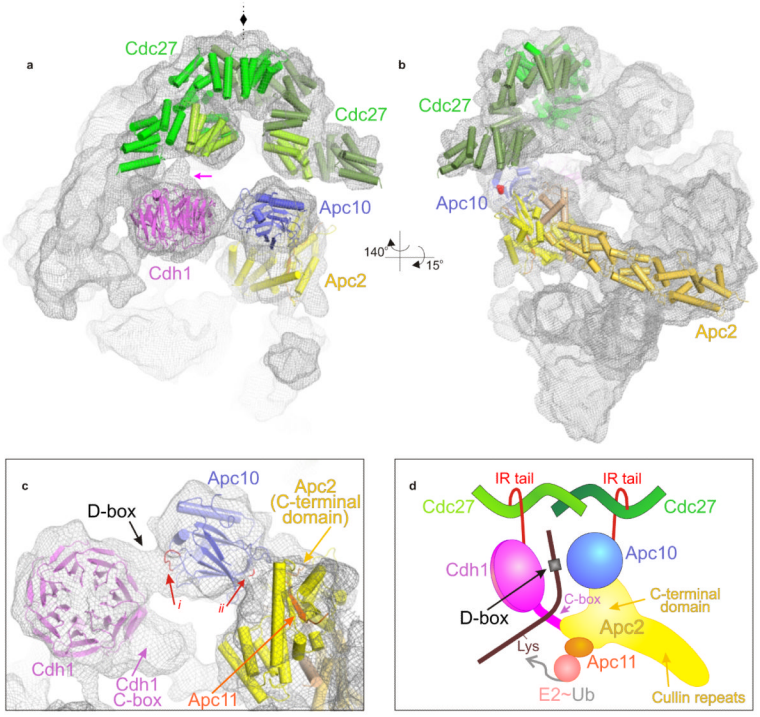

Figure 4.

Cdh1, Apc10, Apc2 and Apc11 form a substrate recognition-catalytic module. (a) and (b). Two views of the cryo-EM APC/C$^{Cdh1\cdot D\text{-}box}$ complex. Protein density is represented by a mesh with fitted atomic coordinates of Cdh1 β-propeller (modelled), Apc10 (ref. [22]), Apc2-Apc11 (modelled on Cul4a-Rbx1 of SCF) and Cdc27 (ref. [26]). Only the N-terminal β-strand of Apc11 bound to the Apc2 CTD is modelled (orange). The two subunits of Cdc27 are shown in light and dark green. View in (a) shows the 2-fold symmetry axis of Cdc27. Density connecting Cdh1 to a TPR-super-helix of the Cdc27 dimer is indicated by an arrow. TPR motifs 8 to 10 of Cdc27, implicated in IR-tail recognition [23], are shown in lighter colourer. In (b) the final residue of Apc10 observed in the crystal structure (Ser 256), 25 residues N-terminal to the IR motif, is indicated by red spheres. (c) Details of the Cdh1 and Apc10 co-receptor for D-box. Both Cdh1 and Apc10 connect to Apc2. The N-terminus of Cdh1, including the C-box linking the WD40 domain to Apc2, is not modelled. Red arrow i denotes the conserved loop (residues His239 to Asp244) of Apc10 implicated in D-box recognition [7], red arrow ii denotes Lys162 and Arg163 of Apc10 responsible for APC/C affinity [7]. Two models for a possible fit of D-box to the density interconnecting Cdh1 and Apc10 are shown in Supplementary Fig. 8. (d) Schematic of combined catalytic and substrate recognition module responsible for D-box binding and substrate ubiquitylation. D-box is represented as binding to an interface between Cdh1 and Apc10.